Dynamic coupling of kinetic and continuum solvers for micro gas flow computations

2014 J. Phys.: Conf. Ser. 501 012029

(http://iopscience.iop.org/1742-6596/501/1/012029)

Journal of Physics: Conference Series **501** (2014) 012029 doi:10.1088/1742-6596/501/1/012029

Dynamic coupling of kinetic and continuum solvers for micro gas flow computations

O Rovenskaya and G Croce
University of Udine, via delle Scienze 208, 33100 Udine, Italy

E-mail: olga.rovenskaya@uniud.it, giulio.croce@uniud.it

Abstract. A hybrid method, dynamic coupling the direct numerical solution of the Bhatnagar-Gross-Krook (BGK) kinetic equation and hydrodynamic Navier-Stokes equations is presented. The decomposition of the physical domain into kinetic and hydrodynamic sub-domains is based on the local Knudsen number and macroparameters gradients. The size of these domains will change during the evolution depending on the current value of the criteria. The solution is advanced in time simultaneously in both kinetic and hydrodynamic domains: the coupling is achieved by matching half fluxes at the interface of the kinetic and Navier-Stokes domains, thus taking care of the conservation of momentum, energy and mass through the interface. Solver efficiency is increased via MPI (Message Passing Interface) parallelization. The accuracy and properties of the proposed method is assessed via successful computation of the flow through a slit, at pressure ratio of 0.5 and for wide range of Knudsen number.

1. Introduction

The coexistence of rarefied continuum flow regime areas and relatively small elements in which rarefaction effects become important is a typical feature of many complex gas flows in micro systems. Thus, kinetic solvers, once limited to niche application in aerospace and vacuum technology, have become of relevant interest for the engineering community. In fact, in micro flows the mean free path of gas molecules is comparable to the characteristic scales of the system. These domains are naturally described by kinetic equation for the velocity distribution function, which involve a considerable effort in terms of CPU time and memory requirements, due to the discretization in both physical and velocity spaces. The continuum domains are well described by the fluid, Euler or Navier–Stokes (NS) equations in terms of average gas flow velocity, gas density and temperature. These equations are more efficient, but less accurate in critical rarefied areas. The development of hybrid solvers combining kinetic and continuum models has, thus, become an important area of research over the last decade. Potential applications of such solvers range from gas flows in micro systems to the aerospace applications, such as high altitude flights. The key parameter defining the choice of the appropriate physical model is related to the local Knudsen number. Major challenges in the development of hybrid code are the identification of kinetic and continuum domains and the choice of the coupling technique.

Different methods presented so far in the open literature can be classified into three categories. The first relies on domain decomposition in physical space: the computational domain is thus decomposed into kinetic and continuum sub-domains using appropriate criteria [1-6]. The second is based on domain decomposition in velocity space, where fast and slow particles are treated separately [7]. The third category includes hybrid models: both kinetic and fluid equations are solved in the entire domain,

using velocity distribution function to compute transport coefficients for the fluid equations [8]. Most of the published works fall into the first category.

Typically, particle methods such as DSMC or Molecular Dynamics are used in regions with strong deviations from equilibrium, and a continuum fluid (Euler or NS, depending on problem features) solver is used elsewhere [3-6]. Nonetheless, the Direct Numerical Solution (DNS) of kinetic equations is a viable alternative to DSMC and may be preferable to DSMC, for coupling purposes, since both kinetic and continuum models use similar numerical techniques. Recent effort to combine DNS with a NS solver used a priori decomposition of the domain, e.g. [2], or combined the DNS of the Boltzmann equation with kinetic schemes of continuum fluid dynamics [1].

The present methodology is a development of the work presented in [2], and requires the decomposition of the physical domain into kinetic and continuum sub-domains by computing gradient-length Knudsen number Kn_{GL}, based on the local Knudsen number and macroparameters gradients [9]. The size of these domains is here dynamically updated during the transient depending on the current Kn_{GL}. The solution is advanced in time simultaneously in both kinetic and continuum domains: the coupling is achieved by matching half fluxes at the interface of the kinetic and NS domains, thus taking care of the conservation of momentum, energy and mass through the interface. This allows the combination of existing in-house codes for numerical solution of both BGK based on the discrete velocity method and a finite-difference finite volume scheme for the NS equations. Furthermore, solver efficiency is increased via MPI (Message Passing Interface) parallelization.

The validation and properties of the proposed approach are assessed via the computation of the gas flow through a slit with both the hybrid and pure kinetic method, for pressure ratio of 0.5 and wide range of Knudsen number. The results are discussed in terms of both accuracy and computational efficiency.

2. Coupling algorithm and numerical methods

The coupling strategy between kinetic and continuum solvers is completely general, and can be applied to the full Boltzmann kinetic equation or its different models and NS or Euler equations. For the sake of simplicity, however, the collision integral is here replaced by the BGK model [10], which can be written as:

$$\frac{\partial f}{\partial t}+\boldsymbol{\xi}\frac{\partial f}{\partial \mathbf{x}}=J_{BGK}(f,f)=\frac{p}{\mu}(M-f) \tag{1}$$

$$M(\rho,\mathbf{V},T)=\rho\left(\frac{m}{2\pi kT}\right)^{3/2}\exp\left[-\frac{m\mathbf{c}^2}{2kT}\right] \tag{2}$$

where $f = f(t, \mathbf{x}, \boldsymbol{\xi})$ is the velocity distribution function, i.e. the probability of finding a molecule with velocity $\boldsymbol{\xi} = (\xi_x, \xi_y, \xi_z)$ in the position $\mathbf{x} = (x, y)$ at the time t. $J_{BGK}(f,f)$ is the collision integral, M is the local Maxwell distribution function, ρ is the gas density, $\mathbf{c} = \boldsymbol{\xi} - \mathbf{V}$ is the relative speed of a single molecule against a background gas with averaged velocity $\mathbf{V} = (u, v)$, p is the local pressure and μ is the viscosity at local temperature T, k is the Boltzmann constant, m is the molecule mass.

The problem is recast in terms of non-dimensional variables using the inlet reservoir equilibrium values as reference ones: density ρ_0, temperature T_0, most probable velocity $v_0 = (2kT_0/m)^{0.5}$, height of the slit H. For the hard-sphere molecular model the non-dimensional viscosity coefficient is $\mu/\mu_0 = (T/T_0)^{0.5}$. Thus, non-dimensional variables are $\boldsymbol{\xi}/v_0$, $\mathbf{x}/H$, $f/(\rho_0 v_0^{-3})$, μ/μ_0, ρ/ρ_0, T/T_0 and p/p_0. For sake of simplicity, in the following the dimensionless quantities keep the same designations as the dimensional ones. In the non-dimensional form the BGK -model equation is thus written as follows:

$$\frac{\partial f}{\partial t}+\boldsymbol{\xi}\frac{\partial f}{\partial \mathbf{x}}=\frac{8}{5Kn_0\sqrt{\pi}}\rho\sqrt{T}\left(M-f\right)=\delta\,\sigma(\rho,T)\left(M-f\right) \tag{3}$$

where $\sigma(\rho, T) = \rho T^{0.5}$, δ is the rarefaction parameter, related to the reference Knudsen number Kn_0 based on the height of the slit H and the mean free path λ_0 at reference conditions:

$$\lambda_0 = \frac{16\mu_0}{5\rho_0}\sqrt{\frac{m}{2\pi k T_0}}, \qquad \delta = \frac{8}{5Kn_0\sqrt{\pi}} \tag{4}$$

The macroscopic density, momentum and internal energy per unit mass, respectively, are defined as:

$$\rho = \int f d\boldsymbol{\xi} \qquad \rho(u,v)^T = \int (\xi_x, \xi_y)^T f d\boldsymbol{\xi} \qquad \rho e = \frac{1}{2}\int \mathbf{c}^2 f d\boldsymbol{\xi} \tag{5}$$

The present approach is based on the idea that NS equations are the first order approximation of the Boltzmann equation, according to the Chapman-Enskog theory [11]. The non-dimensional Chapman–Enskog Navier-Stokes velocity distribution function f_{CE} can be written as:

$$f_{CE} = M\left(1 + Kn_0 f_1\right) \tag{6}$$

$$f_1 = -\frac{1}{p}\left(2\left(c_i c_j - \frac{\mathbf{c}^2}{3}\delta_{ij}\right)\frac{\partial u_i}{\partial x_j} + \frac{\partial T}{\partial x_i}\left(\frac{\mathbf{c}^2}{T} - \frac{5}{2}\right)c_i\right) \tag{7}$$

where f_1 is the correction term and M is the Maxwellian. Substituting f_{CE} in equation (1) and multiplying by the collision vector $\varphi(\boldsymbol{\xi}) = (1, \boldsymbol{\xi}, \boldsymbol{\xi}^2/2)$, integration over the whole velocity domain R^3 recovers the usual conservation laws of mass, momentum and energy:

$$\frac{\partial}{\partial t}\left(\int_{R^3} f_{CE}\varphi^T d\boldsymbol{\xi}\right) + \frac{\partial}{\partial \mathbf{x}}\int_{R^3} f_{CE}\boldsymbol{\xi}\varphi^T d\boldsymbol{\xi} = 0 \tag{8}$$

The use of f_{CE} ensures that equation (8) is equivalent to the usual conservative form of NS equations:

$$\frac{\partial \mathbf{U}}{\partial t} + \frac{\partial \mathbf{F(U)}}{\partial \mathbf{x}} = 0 \tag{9}$$

$$\mathbf{U} = \left(\rho, \rho\mathbf{V}, e + \mathbf{V}^2/2\right)^T = \int f_{CE}\varphi^T d\boldsymbol{\xi} \tag{10}$$

$$\mathbf{F}\left(\mathbf{U}\right) = \int \boldsymbol{\xi}\, f_{CE}\varphi^T d\boldsymbol{\xi} \tag{11}$$

where **U** is the vector of macroscopic values, **F(U)** is the flux.

The choice of switching criterion between kinetic Ω_K and continuum Ω_{NS} regions is important because the wrong domain decomposition could even lead to a non-positive velocity distribution function [5, 9]. In the present work we use gradient-length Knudsen numbers [9]:

$$Kn_{GL\,P} = Kn\frac{\nabla P}{P_{ij\max}} \tag{12}$$

where P represents the parameter of interest, namely density, velocity, or temperature. The actual continuum breakdown parameter is then the maximum of these:

$$Kn_{GL}(x,y) = \max(Kn_{GL\rho}, Kn_{GL\,V}, Kn_{GL\,T}) \tag{13}$$

Schwartzentruber and Boyd [9] suggest that if Kn_{GL} is smaller than a threshold value ε, namely $\varepsilon = 0.05$, the NS equations offer a good approximation of the flow. Thus, at each time step the BGK equation (3) is solved only on a kinetic domain Ω_K, which is a subdomain of physical space (x_i, y_j)

satisfying the condition $Kn_{GL}(x_i, y_j) \geq \varepsilon$. Definition equation (13) is slightly different from the criteria used in [2], based on the norm of the gradient-length Knudsen numbers: in particular, equation (13) provides, for any given flow field and threshold parameter ε, a slightly larger kinetic region and, thus, was here considered better suited to take care of any possible rarefaction effect even during the transients.

The solution of the kinetic equations on a cell *i* requires information on the distribution function for incoming particles from neighbouring cells. On the coupling interface I_c this information has to be provided by the continuum solution; thus, assuming that equation (8) holds true in the continuum subdomain we can impose a Chapman–Enskog distribution, equation (6) :

$$f|_{I_c}(\mathbf{x}) = f_{CE} \qquad \text{if } \boldsymbol{\xi} \cdot \boldsymbol{\vartheta}(\mathbf{x}) < 0 \tag{14}$$

where $\boldsymbol{\vartheta}(\mathbf{x})$ is the outward normal vector to the boundary of Ω_K. Assuming node x_i in the continuum domain and node x_{i+1} in the kinetic one, macroscopic values ρ, $\boldsymbol{V}$, T appearing in $f_{CE}(x_i)$ are computed at the grid point x_i and the evaluation of parameters gradients involves also values in the neighbour to x_i points: x_{i-1}, x_{i+1}.

At solid walls Maxwell diffuse reflecting boundary condition with the full accommodation is applied:

$$f|_w(\mathbf{x}) = \omega(\mathbf{x}) M(1, \mathbf{V}_w, T_w) \qquad \text{if } \boldsymbol{\xi} \cdot \boldsymbol{\vartheta}(\mathbf{x}) < 0 \tag{15}$$

The parameter $\omega(\mathbf{x})$ is determined so as to avoid a mass flux across the wall. All the particles coming off the surface are emitted with the Maxwell distribution functions corresponding the zero mean flow velocity, the temperature is equal to the wall temperature T_w, and the density is calculated from the condition of equality of the fluxes of particles coming on and off the wall. At the symmetry line the specular boundary condition is imposed.

For continuum domain Ω_{NS} we impose total (equilibrium) pressure p_0 and temperature T_0 at inlet region, pressure p_e at exit region. At the coupling interface I_c the following boundary condition is imposed:

$$\mathbf{F}(\mathbf{U}) \cdot \boldsymbol{\vartheta}(\mathbf{x})|_{I_c} = \mathbf{F_i}(\mathbf{U}) \cdot \boldsymbol{\vartheta}(\mathbf{x}) + \mathbf{F_o}(\mathbf{U}) \cdot \boldsymbol{\vartheta}(\mathbf{x}) \tag{16}$$

where $\mathbf{F_i}(\mathbf{U})\ \boldsymbol{\vartheta}(\mathbf{x})$ and $\mathbf{F_o}(\mathbf{U})\ \boldsymbol{\vartheta}(\mathbf{x})$ are the incoming and outcoming half fluxes. Thus, the coupling between kinetic and NS solvers is achieved by imposing the incoming into Ω_{NS} domain half flux $\mathbf{F_i}(\mathbf{U})\ \boldsymbol{\vartheta}(\mathbf{x})$, predicted by the kinetic solver:

$$\mathbf{F_i}(\mathbf{U}) \cdot \boldsymbol{\vartheta}(\mathbf{x}) = \int_{\boldsymbol{\xi} \cdot \boldsymbol{\vartheta}(\mathbf{x}) > 0} \boldsymbol{\xi} \cdot \boldsymbol{\vartheta}(\mathbf{x}) f(t, \boldsymbol{\xi}, \mathbf{x}) \boldsymbol{\varphi}^T d\boldsymbol{\xi} \tag{17}$$

where f is the solution of kinetic equation for molecules exiting from Ω_K. The outcoming flux $\mathbf{F_o}(\mathbf{U})\ \boldsymbol{\vartheta}(\mathbf{x})$ from Ω_{NS} to Ω_K domain is defined as:

$$\mathbf{F_o}(\mathbf{U}) \cdot \boldsymbol{\vartheta}(\mathbf{x}) = \int_{\boldsymbol{\xi} \cdot \boldsymbol{\vartheta}(\mathbf{x}) < 0} \boldsymbol{\xi} \cdot \boldsymbol{\vartheta}(\mathbf{x}) f_{CE}(t, \boldsymbol{\xi}, \mathbf{x}) \boldsymbol{\varphi}^T d\boldsymbol{\xi} \tag{18}$$

It can be seen, that the NS model acts on the kinetic one by imposing the incoming Chapman–Enskog function f_{CE} on the coupling interface I_c, while the macroscopic parameters ρ, $\mathbf{V}$, T and their gradients for f_{CE} are computed locally.

2.1. Numerical scheme for the BGK equation

Taking advantage of the two-dimensionality of the flow, the *z* component of the molecular velocity may be eliminated by the projection procedure. For the sake of simplicity a scheme will be written for general BGK- model equation (3).

To discretize the BGK-model equation we construct in velocity space a two-dimensional grid $\{\boldsymbol{\xi}_\boldsymbol{\Gamma}\} = (\xi_{x\alpha}, \xi_{y\beta})$, $\alpha, \beta = 1, \ldots, N_\xi$ bounded by $v_{\max}$, where $\boldsymbol{\Gamma} = (\alpha, \beta)$ defines velocity grid points indices.

Velocity space nodes are located at Gaussian abscissas, and Gaussian integration is performed via proper Gaussian weight function. In the discrete form the BGK-model equation (3) is the following:

$$\partial_t f_{\mathbf{\Gamma}} + \xi_{x\mathbf{\Gamma}} \frac{\partial f_{\mathbf{\Gamma}}}{\partial x} + \xi_{y\mathbf{\Gamma}} \frac{\partial f_{\mathbf{\Gamma}}}{\partial y} = \delta\sigma(\rho, T)\left(M_{\mathbf{\Gamma}} - f_{\mathbf{\Gamma}}\right) \tag{19}$$

In the physical space a 2D, non uniform grid is defined by nodes (x_i, y_j), for $i = 1, i_{max}$ and $j = 1, j_{max}$ and $N_c = i_{\max} \cdot j_{\max}$ cells centred around each node. Denoting $f^n_{\mathbf{\Gamma},i,j}$ as the approximations of $f(t^n, \xi_{\mathbf{\Gamma}}, x_i, y_j)$ the explicit-implicit numerical scheme for the equation (19) can be written as [12]:

$$f^{n+1}_{\mathbf{\Gamma},i,j} = \frac{1}{1+\delta\sigma^{n+1}\Delta t}\left(f^n_{\mathbf{\Gamma},i,j} - \Delta t \xi_{x\mathbf{\Gamma}} \frac{\partial f^n_{\mathbf{\Gamma},i,j}}{\partial x} - \Delta t \xi_{y\mathbf{\Gamma}} \frac{\partial f^n_{\mathbf{\Gamma},i,j}}{\partial y} \right) + \frac{\delta\sigma^{n+1}\Delta t}{1+\delta\sigma^{n+1}\Delta t} M^{n+1}_{i,j} \tag{20}$$

The transport term in equation (20) is treated explicitly and approximated by a standard finite volume scheme. In particular, the numerical fluxes are determined by the third order MUSCL with the Van Albada limiter. The time step should be limited by the condition:

$$\Delta t_K = CFL / \max_{ij}\left(v_{\max}/\Delta x + v_{\max}/\Delta y\right) \tag{21}$$

The equation (20) is solved on a curvilinear, structured mesh. If we define curvilinear coordinates $\zeta(x, y)$ and $\eta(x, y)$ and a uniform grid $\varsigma_i = i\Delta\varsigma$, $\eta_j = j\Delta\eta$ a scheme very similar (20) may be used.

Since the kinetic part is time consuming, the code is parallelized in order to improve its efficiency. The solution of system (20) is local in $\mathbf{\Gamma}$, and therefore completely parallelizable in velocity space. The software code was written in C++ with the use of MPI.

2.2. Numerical scheme for the Navier–Stokes equations

The flux vector in equation (9) **F(U)** may be decomposed into the convective (inviscid) and diffusive (viscous) components:

$$\mathbf{F} = \mathbf{F}^{\mathbf{inv}} - \mathbf{F}^{\mathbf{v}} \tag{22}$$

$$\mathbf{F}^{\mathbf{inv}} = \left(\rho\mathbf{V}, \rho\mathbf{V}\mathbf{V} + p\mathbf{I}, \mathbf{V}(e + \mathbf{V}^2/2 + p)\right)^T \tag{23}$$

$$\mathbf{F}^{\mathbf{v}} = \left(0, \boldsymbol{\tau}, \boldsymbol{\tau}\cdot\mathbf{V} + \mathbf{q}\right)^T \tag{24}$$

where **I** is the identity matrix and **q** is the heat flux vector

Navier-Stokes solver is based on a hybrid finite difference-finite volume method and has formal second order accuracy in space and time [2]. Fluxes are defined via neighbouring value averaging, and an artificial dissipation term is added to prevent checker boarding and numerical instabilities. Artificial dissipation terms are given by a blend of second and fourth order differences, scaled by the maximum eigenvalue of jacobian matrix of vectors $\mathbf{F}^{\mathbf{inv}}$, as suggested in [13]. Second order terms are switched on near discontinuities. Viscous flux vectors are evaluated with second order finite differences at i+1/2. The solution is advanced in time via Crank Nicolson integration scheme. The use of the spatially factored ADI scheme originally proposed by Beam and Warming leads, at each time step, to the resolution of two series of block tridiagonal algebraic systems, rather than the original pentadiagonal block system arising from flux discretization.

At the solid wall the Maxwell first order slip boundary condition is used:

$$u_{gas} - u_w = s_p Kn\left(\frac{\partial u_{\eta(\mathbf{x})}}{\partial\varsigma(\mathbf{x})} + \frac{\partial u_{\varsigma(\mathbf{x})}}{\partial\eta(\mathbf{x})}\right) \qquad s_p = \frac{\sqrt{\pi}}{2}\frac{2-\sigma_v}{\sigma_v}\left(1 + 0.1366\sigma_v\right) \tag{25}$$

where $\varsigma(\mathbf{x})$ and $\eta(\mathbf{x})$ are the unit vectors respectively normal and tangential to the solid wall. σ_v is the tangential momentum accommodation coefficient, here chosen equal to one, thus in the computations s_p is close to one. The additional derivative along the tangential direction is essential in capturing even the qualitative behaviour of slip flow along curved walls.

A Dirichlet temperature boundary condition is imposed at the wall. Namely, the wall temperature is fixed at the inlet total temperature value to minimize the effect of viscous dissipation. In the energy equation, the Smoluchowski temperature jump is used:

$$T_{gas} - T_w = s_T Kn \frac{\partial T}{\partial \eta(\mathbf{x})}, \; s_T = \frac{2-\sigma_T}{\sigma_T} \frac{2\gamma}{\gamma+1} \frac{1}{\mathrm{Pr}} \tag{26}$$

where s_T is the temperature jump coefficient. Since isothermal flow is considered we assume the temperature accommodation coefficient σ_T equals to one.

3. Results and discussion

The two-dimensional flow of a gas through a slit of height H cut in an infinitely thin partition separating two containers is considered. The gas in the containers, far from the slit, is in equilibrium at temperature T_0 and pressures p_0 and $p_e = 10^5$ Pa, with $p_0 > p_e$. The slit is considered as infinite in the z direction. Since the flow is symmetric about $y = 0$, therefore, only a half of the flow, shown in figure 1, will be considered. Two large computational areas of radius R before and after the slit ($-H/2 \le y \le 0$) are included in the computational domain, simulating the upstream and downstream reservoirs. I_c is the interface between inner kinetic sub-domain and outer NS one.

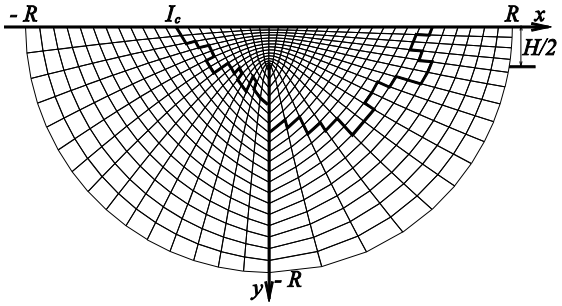

Figure 1. Computational domain sketch.

The gas flows due to a pressure difference p_e/p_0 between upstream and downstream reservoirs. The static inlet pressure p_i is the result of computation, although, due to the low inlet velocities, it almost coincides with p_0. The gas flow through the slit is also determined by the rarefaction parameter δ.

The global characteristic of the flow, dimensionless flow rate W, is introduced as:

$$W = \frac{\dot{m}}{\dot{m}_{fm}} \qquad \dot{m}_{fm} = \frac{p_0}{\sqrt{\pi} v_0} \tag{27}$$

where $\dot{m}_{fm}$ is the analytically deduced mass flow rate in the limit of free molecular regime and the mass flow rate through the slit are computed as:

$$\dot{m} = 2\int_{-1/2}^{0} \rho(0,y) u(0,y) dy \tag{28}$$

The use of circular sectors as plenum, rather than the more common square shape, allows reservoirs of large size with a relatively smaller number of grid points, while preserving a strong refinement near the slit. The accuracy of the numerical results is sensitive to the sizes of the left and right reservoirs: in [2] it was shown that the radius $R = 40H$ is sufficiently large for correct computations.

A non uniform curvilinear grid of 160 nodes in the streamwise direction with minimum grid spacing $0.017H$ and 40 nodes in the transverse direction is used (see figure 1). Grid independence test has been done using the finer grid with 240 × 40 nodes. The mass flow difference between fine and coarse meshes is less than 1%. In the velocity space a 24 × 24 grid is implemented. An increase in the velocity grid points of 64% led to a 1% change in global mass flow.

Since time step is unique for both solvers, it should satisfy the stricter stability (or accuracy) constraint $\Delta t = \min(\Delta t_K, \Delta t_{NS})$. The iteration process is terminated when a relative convergence criterion of 10^{-7} imposed on the non-dimensional flow rate is fulfilled.

The code ran on double processors, quad core systems, using thus up to 8 parallel processes. The CPU time of the hybrid solver is basically determined by the kinetic one and the advantage depends essentially on the ratio between the number of grid nodes on the (expensive) kinetic domain and the number of grid nodes in the (cheap) NS one.

To illustrate effect of switching criteria ε on the computed flow field, we show non dimensional mass flow rate W_h obtained by hybrid simulations for δ = 1 (see table 1). For large ε, the mass flow rate is quite different from the BGK kinetic value, $W_{BGK} = 0.653$. The mass flow rate W_h converges to the correct value when the switching parameter ε decreases below 0.1.

Table 1. Non-dimensional mass flow rate δ = 1.

ε	W_h	W_{BGK}
0.05	0.653	
0.1	0.653	
0.5	0.640	0.653
1	0.621	
2	0.591	

The CPU time per time step of hybrid code is dictated by the time for solving the BGK equation, since the sum of CPU time relative to NS solutions and coupling computations is quite small, relatively to the kinetic solution requirements, at least in the field of interest (i.e., as will be shown, δ<20). For example, if whole domain is considered as kinetic (160 × 40 points) the CPU time is 1.6 s, more than an order of magnitude longer than a full NS time step, while for δ = 100 (approximately 160 kinetic nodes) the CPU time is 0.28 s; for δ = 10 (3000 kinetic nodes) the CPU time is 0.93 s; for δ = 5 (4100 kinetic nodes) the CPU time is 1.2 s.

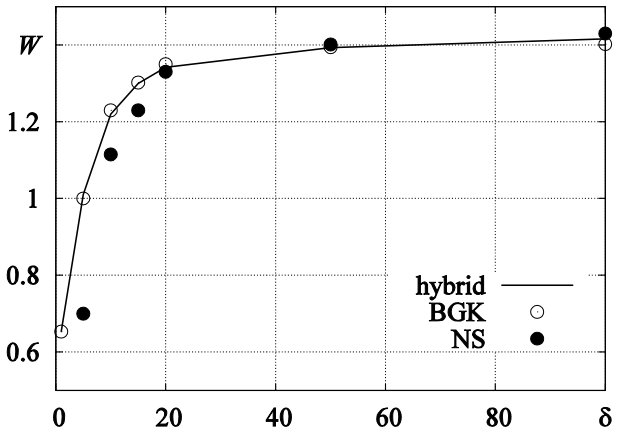

Figure 2. Non-dimensional mass flow rate via δ.

It should be mentioned that parallelization in velocity space allow us to uniformly distribute kinetic points between processors. Each processor works with the same number of kinetic points in physical space. Now the speed up of hybrid code is around 82% was reached for $\delta = 100$ and 25% for $\delta = 5$, but further improvements of code are still possible. An even higher speed up ratio is expected in case the Boltzmann collision integral is used instead BGK model, since the coupling overhead become completely negligible.

In figure 2, non-dimensional flow rates are compared with results computed by the pure BGK and NS solvers for the pressure ratio of 0.5 and rarefaction parameter δ ranging from 1 to 100. For $\delta \geq 20$ mass flow rates obtained by hybrid, BGK and NS solvers are close to each other (maximum difference is less than 2.5%). For smaller δ the difference between NS and BGK flow rates becomes higher and for $\delta = 5$ is around 45%, while hybrid code reproduces mass flow close to kinetic data.

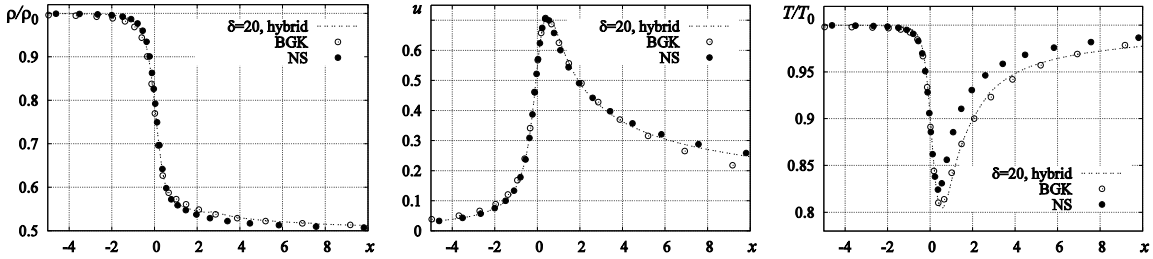

Figure 3. Density ρ/ρ_0, axial velocity u and temperature T/T_0 along the symmetry axis $y = 0$, $\delta = 20$.

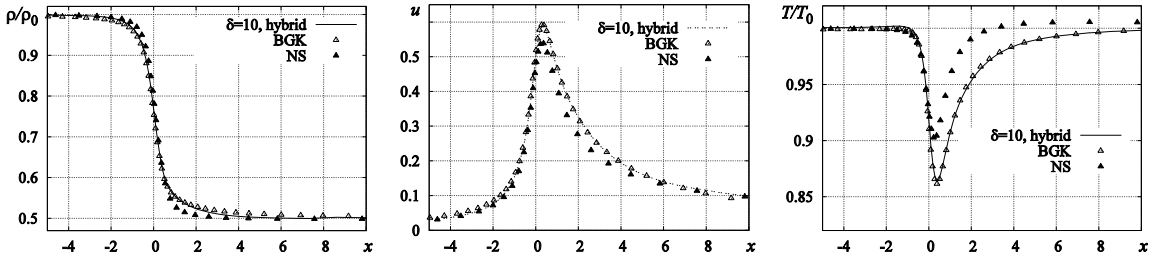

Figure 4. Density ρ/ρ_0, axial velocity u and temperature T/T_0 along the symmetry axis $y = 0$, $\delta = 10$.

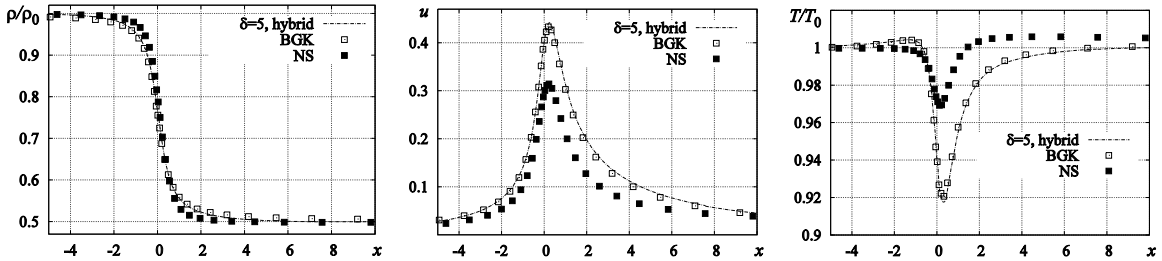

Figure 5. Density ρ/ρ_0, axial velocity u and temperature T/T_0 along the symmetry axis $y = 0$, $\delta = 5$.

The variations of the dimensionless density, temperature, normalized by the inlet values, and velocity along the symmetry axis are shown in figures 3-5 for rarefaction parameters 20, 10 and 5. Coupled solutions are compared with BGK and NS results. Density (or pressure) variations are qualitatively similar in all cases. Before and after the slit density tends to upstream and downstream conditions, while in the slit region it sharply decreases. The axial velocity far upstream is almost zero and it grows in the region around the slit. The velocity increase is smaller at larger rarefaction (smaller δ). The temperature decreases near the slit, while at the rest of the domain it remains very close to the reference temperature. The temperature drop is larger as δ increases. The coupled solutions are close enough to the kinetic ones for all values of rarefaction parameters.

The contour lines of density and Mach number (solid line) near the slit region for different rarefaction are presented in figures 6-8, together with the extension of the kinetic region at convergence (dashed line).

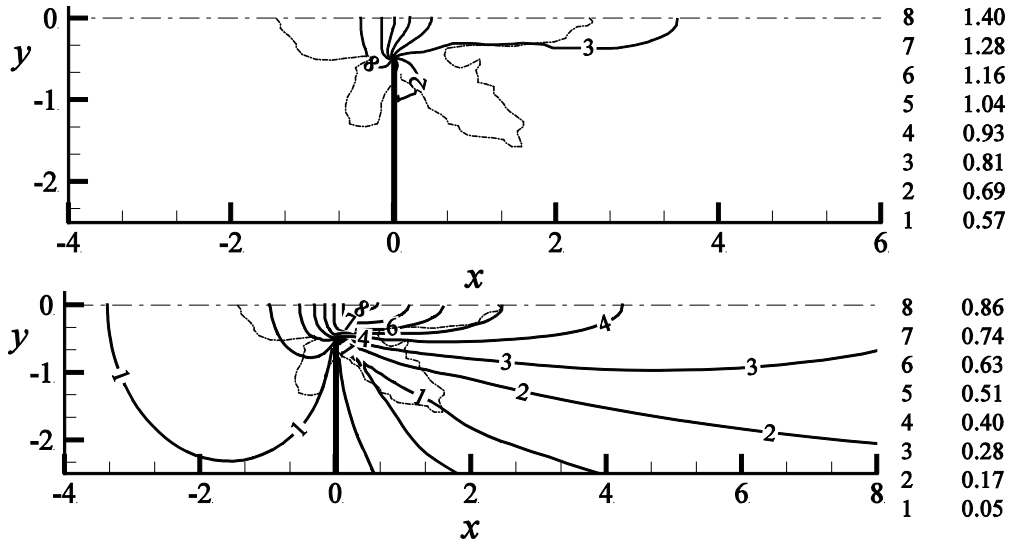

Figure 6. Dimensionless density (top) and Mach number (bottom) near the slit: δ = 20.

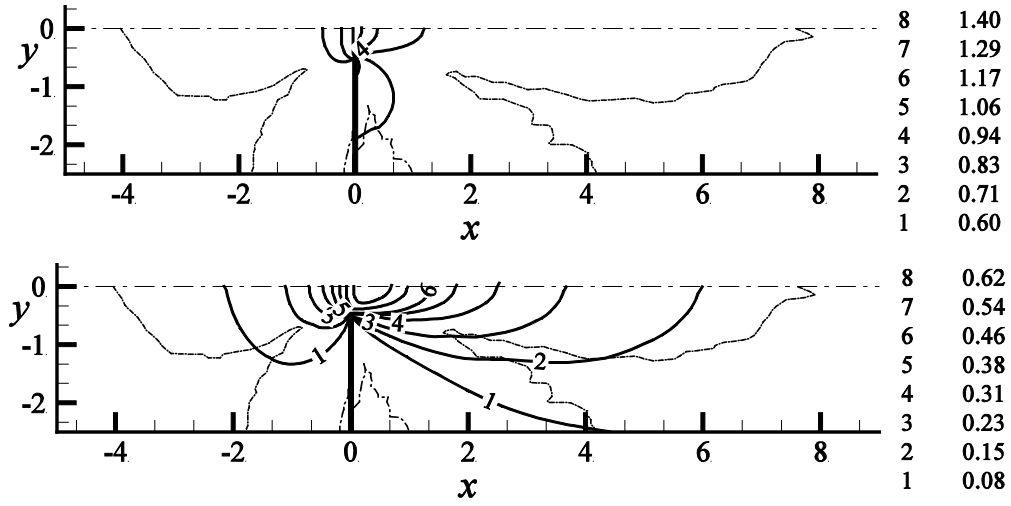

Figure 7. Dimensionless density (top) and Mach number (bottom) near the slit: δ = 10.

For small rarefaction δ = 20 (figure 6) the local Knudsen number near the coupling boundary varies from 0.07 to 0.11. The coupling between kinetic and NS solutions shows a smooth transition along the contour lines crossing the domains interface, especially for the Mach number contour.

Finally, to assess the possibility of hybrid code, the case δ = 5 is shown in figure 8. At the coupling interface the local *Kn* rise up to 0.1; furthermore, its maximum value occurs close to the slit (within the kinetic domain) and is equal to 0.4. NS solution would not, thus, be appropriate for the solution over the whole domain as can be seen in figure 5. The flow solution has now more relevant viscous effects, which smooth the transonic flow structures. Nevertheless, the hybrid solver gives a good prediction of mass flow (see figure 2) and the contour lines crossing domains still appear smooth and regular.

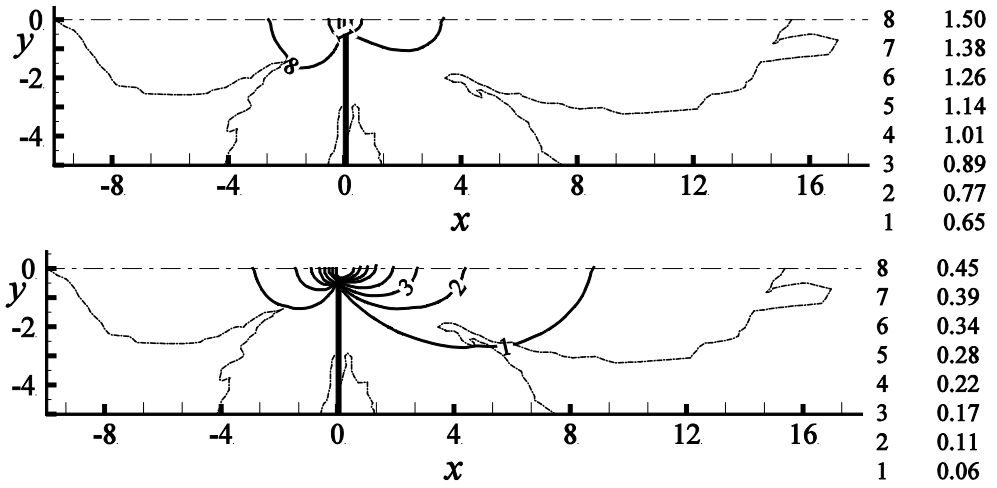

Figure 8. Dimensionless density (top) and Mach number (bottom) near the slit: $\delta = 5$.

4. Conclusion

A hybrid algorithm based on the direct numerical solution of the BGK kinetic equation coupled to a Navier-Stokes model was presented. The solution is advanced in time simultaneously in both kinetic and continuum domains: the coupling is achieved by matching half fluxes at the interface of the kinetic and NS domains, taking care of the conservation of momentum, energy and mass through the interface, and is flexible enough to allow for the use of existing solver on both sides. Mass flow rates and flow parameters are close to full BGK solutions. The capability of the hybrid code to simulate the gas flow through slit for a wide range of Knudsen number, exceeding the range of applicability of pure Navier-Stokes, has been demonstrated. The CPU time savings, with respect to a full BGK solutions, are significant, although strongly depends on the size of the kinetic region.

It should be noticed that the dynamic coupling is more effective then static one, allowing to capture and describe properly the kinetic regions even when they appear, during the convergence transient, in areas not easy to predict a-priori. This allows to get satisfying results even for relatively high Knudsen.

Acknowledgments

The research leading to these results has received partially founding from MIUR grant (PRIN 2009).

References

[1] Kolobov V I, Arslanbekov R R, Aristov V V, Frolova A A, Zabelok S A 2007 *J. of Comput. Phys*. **223** 589–608.
[2] Rovenskaya O, Croce G 2013 *Heat Transfer Eng.* **34** 192-203.
[3] Le Tallec P, Mallinger F J 1997 *Comput. Phys.* **136** 51-67.
[4] Tiwari S 1998 *J. Comput. Phys.* **144** 710-726.
[5] Carlson H A, Roveda R, Boyd I D, Candler G V 2004 AIAA 2004-1180.
[6] Wijesinghe H S, Hornung R, Garsia A L, Hadjiconstantinou H N 2004 *J. Fluids Eng.* **126** 768–777.
[7] Crouseilles N, Degond P, Lemou M 2004 *J. Comput. Phys.* **199** 776-806.
[8] Beylich A E 2000 *Phys. Fluids* **12** 444–465.
[9] Schwartzentruber T E, Boyd I D 2006 *J. of Comput. Phys*. **215** 402–416
[10] Bhatnagar P L, Gross E P, Krook M A 1954 *Phys. Rev.* **94** 511-525.
[11] Chapman S, Cowling T G 1990 *The mathematical theory of nonuniform gases* (Cambridge: Univ. Press).
[12] Filbet F, Jin S 2010 *J. of Comput. Phys.* **229** 7625-7648.
[13] Pulliam T H 1986 *AIAA Journal* **24** 1931-1940